Taylor & Francis
Taylor & Francis Group

Numerical Solution of a Three-Phase Stefan Problem with High Power Input

GUIDO PARISSENTI and ALFONSO NIRO

Politecnico di Milano, Dipartimento di Energia, Milano, Italy

The numerical solution of a one-dimensional, three-phase Stefan problem with a low Stefan number is presented. Joule heating and thermal radiation are demonstrated to be negligible compared to the high power input. The front tracking method is used along with a second-order Lagrangian interpolation of the temperature profile near the moving surface defined by the location of the phase change. Results are compared with analytical, numerical, and experimental solutions available in literature.

INTRODUCTION

Being vacuum the best dielectric it is obvious its application in technological situations involving high current levels to be shut off safely and as instantaneously as possible. Vacuum switches apply this principle, and for this reason they have a key role in many high power electrical systems. One of the problems affecting such devices is the appearance of electric arcs between the electrodes due to the sometimes extremely high current level involved. Arcs happen because absolute vacuum is not achievable and a few electric carriers are always present. The intense heat fluxes of arcs can damage switches by melting the electrodes locally. In fact, these phenomena happen in small zones that appear like small spots after the arc. These spots, with different shapes and dimensions, can be found on either electrode, causing erosion.

Because spots appear to be a key element in understanding arc formation and extinction, a Stefan multiphase thermal model of the spot formation is presented here. Historically, for this kind of problem very few analytical solutions have been found and only for the simplest cases with no more than two phases [1, 2], applied for infinite or semi-infinite regions. The same solution can instead be easily obtained numerically [3] with the possibility of solving more difficult problems [4]. Three-phase problems

have been already solved numerically in the past [5], but using complex and rigid finite-element methods, unsuitable to be inserted into larger codes for the simulation of complex physical problems involving not exclusively thermal phenomena. Hence the purpose of this paper is to describe the application of a common finite-difference technique coupled with the front tracking method to this complex multiphase problem. We show the flexibility of the formulation, as well as that the results obtained are in good agreement with the literature. Due to its simplicity and low computation time, the presented approach can be used to preliminary evaluate damages occurring on electrode surfaces during initial sizing and design of vacuum switches. In addition, the presented method can be applied to every application that involves concentrated high-power deposition on surfaces, that is, electric thrusters for in-space propulsion or even laser ablation. More complex and multidimensional methods can be successively applied to increase the detail of the solution [6–8].

PHYSICAL DESCRIPTION OF THE THERMAL MODEL

Spots are small craters formed by an electric arc onto the electrode surface and they are usually round with a melted internal surface. The image in Figure 1 shows some spots cratered by an arc with a current density on the order of $10^9 A/m^2$ on an aluminum anode.

Single spots from high-current electric arcs usually are much smaller than the electrode where they form [9–12]. In addition, the depth of the spot is much smaller, at least three times, than

Address correspondence to Professor Alfonso Niro, Politecnico di Milano, Dipartimento di Energia, Via Lambruschini 4, 20156 Milano, Italy. E-mail: alfonso.niro@polimi.it
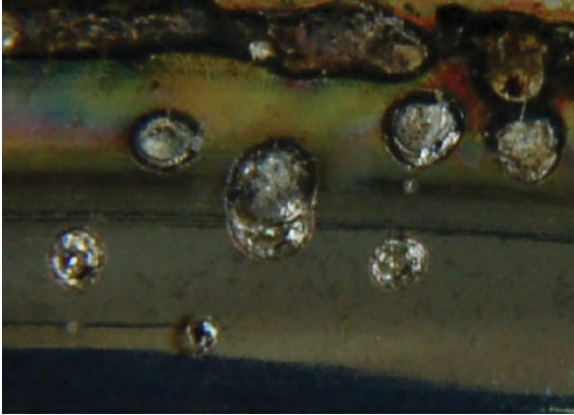
Figure 1 Spots on aluminum anode.

its diameter [9, 12]. From an analytical point of view, Lehr and Kristiansen [13] show that if the diffusion length $(\alpha_s t_d)^{1/2}$ is four times smaller than the electrode thickness by the incident heat flux direction, the electrode itself can be considered infinite in extent (t_d is a phenomenon characteristic time like the total

discharge time, e.g., near 1 ms). For copper this leads to a diffusion length of 0.35 mm, much smaller than the thickness of a typical electrode. Therefore, the problem can be considered as one-dimensional. A schematic representation of the model is shown in Figure 2 and it can be mathematically described by the following set of equations.

Heat diffusion equations:

$$k_s \frac{\partial^2 T_s}{\partial X^2} + \eta_s j^2 = \rho c_s \frac{\partial T_s}{\partial t} \quad \text{for} \quad S_1 < X < a \qquad (1)$$

$$k_l \frac{\partial^2 T_l}{\partial X^2} + \eta_l j^2 = \rho c_l \frac{\partial T_l}{\partial t} \quad \text{for} \quad S_2 < X < S_1 \qquad (2)$$

Stefan equations on moving surfaces:

$$k_s \frac{\partial T_s}{\partial X} - k_l \frac{\partial T_l}{\partial X} = \rho C_m \frac{dS_1}{dt} \quad \text{for} \quad X = S_1, t > t_1 \qquad (3)$$

$$k_l \frac{\partial T_l}{\partial X} + F(t) = \rho C_v \frac{dS_2}{dt} \quad \text{for} \quad X = S_2, t > t_2 \qquad (4)$$
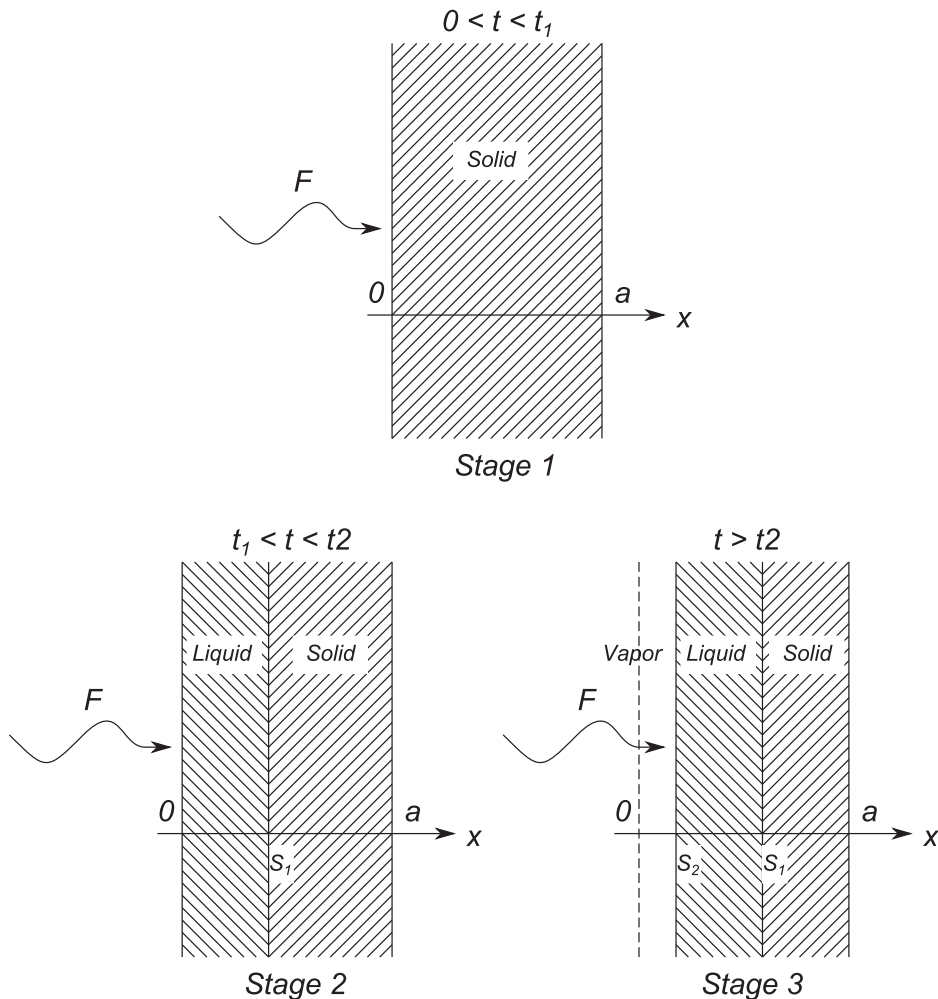

Figure 2 Stages of the model.

Initial conditions:

$$T_s = T_i \quad \text{for} \quad t = 0 \tag{5}$$

$$S_1 = 0 \quad \text{for} \quad t < t_1 \tag{6}$$

$$S_2 = 0 \quad \text{for} \quad t < t_2 \tag{7}$$

Boundary conditions:

$$T_s = \quad T_i \qquad \text{for} \quad X = a \tag{8}$$

$$-k_s \frac{\partial T_s}{\partial X} = \quad F(t) \qquad \text{for} \quad X = 0, t < t_1 \tag{9}$$

$$-k_l \frac{\partial T_l}{\partial X} = \quad F(t) \qquad \text{for} \quad X = 0, t_1 < t < t_2 \tag{10}$$

$$T_s = T_l = T_m \quad \text{for} \quad X = S_1, t > t_1 \tag{11}$$

$$T_l = \quad T_v \qquad \text{for} \quad X = S_2, t > t_2 \tag{12}$$

The model can be described as a semi-infinite solid (approximate as a slab of length $a \gg (\alpha_s t_d)^{1/2}$) in the region $X > 0$, where X is the spatial coordinate perpendicular to the surface, where the heat flux $F(t)$ is applied at $X = 0$. Additional terms for radiation as well as for Joule heating are also considered. The $F(t)$ flux first raises the solid temperature to the melting value T_m (Stage 1). At this time t_1 a new phase appears with a new domain for the liquid phase. Hence, the original slab is split into two different time-varying domains. While the surface S_1 is moving following Eq. (3), the temperature in the liquid phase starts rising until the vaporization temperature T_v is attained at $t = t_2$ (Stage 2). At this time, the surface S_2 appears and starts moving following a relation similar to those for S_1 (Stage 3).

We assume all thermal properties of the electrode are constant. Although in the vapor phase a temperature profile does not exist because vapor is assumed to be removed as soon as it forms, in the solid and liquid phases the temperature dynamic is ruled by the heat diffusion equations. At each moving surface, the Stefan equation (described by Eqs. (3) and (4)) is introduced, to take into account the energy balance between the heat flux coming from the two phases and the change in internal energy due to the melting or vaporization. For the numerical solution, obviously, it is not possible to consider a semi-infinite domain, so we consider the solid as a slab in the domain $0 < X < a$ with $a \gg r_d$. Because of this hypothesis, we assume that at $X = a$ temperature should always remain equal to the initial temperature T_i, and temperature gradient is null. The verification of these conditions means that the region remains unchanged; nevertheless, only one of the two conditions (Dirichlet or Neumann—null temperature gradient) can be imposed; fixing one of these two boundary conditions at $X = a$ in the finite differences code is only a matter of choice, as both should be verified after the simulation, to check whether a has been taken sufficiently large. We decided to impose the Dirichlet condition, except in comparing to other codes, where the test case condition was used.

Liquid and solid are considered to have the same density ρ to allow a simpler manipulation of the Stefan equations and to avoid thermal expansion. The error is no larger than around 10% for both copper and aluminum.

FINITE DIFFERENCES DISCRETIZATION AND FRONT TRACKING METHOD

The most difficult issue in using a finite-difference method for this kind of problem is the time dependence of the domains. We cannot assume the moving boundaries always lie on a node of the mesh, and therefore we do not have a unique domain. Considering two separate domains with different discretizations is also difficult, because at the beginning of the simulation one of them will be very small or null. To bypass these problems is it possible to use the front tracking method [2]. The positions S_1 and S_2 of the moving boundaries are obtained from the integration of the Stefan equations (3) and (4), and therefore are not required to be a multiple of the mesh size. Let us say that at any simulation time step the phase-change boundary is located between two consecutive grid points, for example, $i\delta X$ and $(i + 1)\delta X$. To be able to define the finite difference form of the heat transfer equations (1) and (2) for these two points, we need to use a second-order Lagrangian interpolation to allow unequal spatial intervals. We show that the appearance of the solid–liquid boundary requires us to lower the order of the interpolation to 1 for the initial step because the domain is restricted to only one node.

As previously mentioned, this model considers heat generation and thermal radiation. The former is the term ηj^2 in Eqs. (1) and (2) due to the current that flows into the spot and resistively heats the material. The thermal radiation can be considered in a very simple way by dividing $F(t)$ into two parts:

$$F(t) = \tilde{F}(t) - q_r(t) \quad \text{where} \quad q_r(t) = \sigma\varepsilon\left(T_{surf}^4 - T_i^4\right)$$

where $q_r(t)$ is the heat flux that leaves the external surface (solid or liquid, depending on the phase status). $\tilde{F}(t)$ can be considered the external heat flux that flows into the anode, depending on the physics of the problem.

Nondimensionalization

The first operation is the nondimensionalization of the equations. The advantages to this operation are a simplification in writing the finite-difference form and the ability to obtain the Stephan number, a dimensionless value that gives information about the problem dynamics. Some characteristic parameters are chosen for this operation:

$$\begin{aligned} x = \frac{X}{r} \qquad x_{s,l} = \frac{X_{s,l}}{r} \qquad s_{1,2} = \frac{S_{1,2}}{r} \\ \tau = \frac{k_s t}{c_s \rho r^2} \\ u_s = \frac{T_s}{T_m} \qquad u_l = \frac{T_l}{T_m} \qquad u_v = \frac{T_v}{T_m} \end{aligned} \tag{13}$$

All the symbols are explained in the Nomenclature section.

Substituting these dimensionless variables into Eqs. (1) and (2) we have:

$$\frac{\partial^2 u_s}{\partial x^2} + g_s = \frac{\partial u_s}{\partial \tau} \quad \text{for} \quad s_1 < x < \frac{a}{r} \quad (14)$$

$$\frac{\partial^2 u_l}{\partial x^2} + g_l = \tilde{k}\frac{\partial u_l}{\partial \tau} \quad \text{for} \quad s_2 < x < s_1 \quad (15)$$

where

$$\tilde{k} = \frac{k_s}{k_l}\frac{c_l}{c_s} \qquad g_s = \frac{\eta_s\, j^2 r^2}{k_s T_m} \qquad g_l = \frac{\eta_l\, j^2 r^2}{k_l T_m}$$

Equations (3) and (4) can be manipulated in the same way:

$$Ste\frac{\partial u_s}{\partial x} - \gamma_l\frac{\partial u_l}{\partial x} = \frac{ds_1}{d\tau} \quad \text{for} \quad x = s_1, \tau > \tau_1 \quad (16)$$

$$\gamma_{lv}\frac{\partial u_l}{\partial x} + f(\tau) = \frac{ds_2}{d\tau} \quad \text{for} \quad x = s_2, \tau > \tau_2 \quad (17)$$

where

$$\gamma_l = \frac{k_l\, Ste}{k_s} \qquad Ste = \frac{c_s T_m}{C_m}$$

$$\gamma_{lv} = \frac{k_l\, \lambda_v}{k_s} \qquad f(\tau) = \frac{F(t)r\lambda_v}{k_s T_m} \qquad \lambda_v = \frac{c_s T_m}{C_v}$$

The Stefan number Ste expresses the importance of sensible heat relative to latent heat. For metals like aluminum, copper, tin, and other, the Stefan number is small, in the order of unity. This means that the heat released or absorbed by the interface during phase change is mostly unaffected by the variation of internal thermal energy of the material [14]. The boundary and initial conditions can be transformed as follows:

$$u_s = u_i \quad \text{for} \quad x = \frac{a}{r} \quad (18)$$

$$\frac{\partial u_s}{\partial x} = -f_s(\tau) \quad \text{for} \quad x = 0, \tau < \tau_1 \quad (19)$$

$$\frac{\partial u_l}{\partial x} = -f_l(\tau) \quad \text{for} \quad x = 0, \tau_1 < \tau < \tau_2 \quad (20)$$

$$u_s = u_l = u_B = 1 \quad \text{for} \quad x = s_1 \quad (21)$$

$$u_l = u_v \quad \text{for} \quad x = s_2 \quad (22)$$

$$u_s = u_i \quad \text{for} \quad \tau = 0 \quad (23)$$

$$s_1 = 0 \quad \text{for} \quad \tau < \tau_1 \quad (24)$$

$$s_2 = 0 \quad \text{for} \quad \tau < \tau_2 \quad (25)$$

where

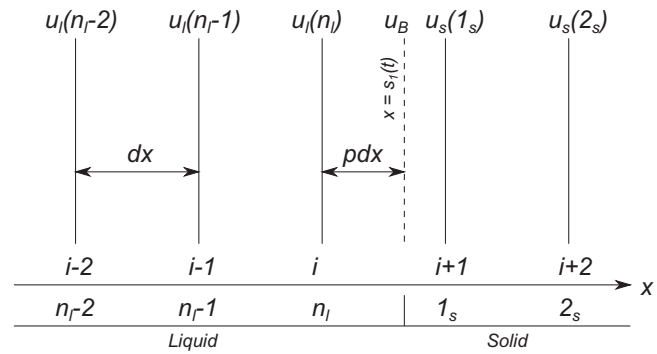$$f_s(\tau) = \frac{F(t)r}{k_s T_m} \qquad f_l(\tau) = \frac{F(t)r}{k_l T_m}$$

Figure 3 Lagrangian-type interpolation for solid–liquid boundary.

Lagrangian-Type Interpolation

The Lagrangian-type interpolation method used by Crank [2] allows a modification of the finites difference formulae incorporating unequal spatial intervals near the moving boundary. Using a second-order scheme based on three points, a generic function $u(x)$ can be represented as

$$u(x) = \sum_{j=0}^{2} l_j(x)u(a_j) \quad (26)$$

$$l_j(x) = \frac{p_2(x)}{(x - a_j)\dfrac{dp_2(x)}{dx}\bigg|_{x=a_j}} \qquad p_2(x) = (x-a_0)(x-a_1)(x-a_2)$$

$$(27)$$

where $u(a_0)$, $u(a_1)$, and $u(a_2)$ are three known values of $u(x)$ at the points $x = a_0, a_1, a_2$. From $u(x)$, is it possible to obtain the first and second derivatives expressed in terms of a_j.

Referring to Figure 3, where the moving boundary between liquid and solid is shown to be at a fractional distance pdx from the considered node i, it is possible to specialize the preceding formulas to obtain the derivative in these two spatial intervals. Substituting values for a_j and $u(a_j)$, pertaining to the solid phase,

a_j	$u(a_j)$
$a_0 = (i + 1 - (1 - p))dx = (i + p)dx$	u_B
$a_1 = (i + 1)dx$	$u_s^{i+1} = u_s^1$
$a_2 = (i + 2)dx$	$u_s^{i+2} = u_s^2$

we write the derivatives

$$\frac{\partial^2 u_s}{\partial x^2} = \frac{1}{dx^2}\left(\frac{u_B}{(1-p)(2-p)} - \frac{u_s^1}{1-p} + \frac{u_s^2}{2-p}\right) \quad (28)$$

for $x = (i + 1)\,dx$, the first node of the solid domain, and

$$\frac{\partial u_s}{\partial x} = \frac{1}{dx}\left(\frac{2-3p}{(1-p)(2-p)}u_B + \frac{2-p}{1-p}u_s^1 - \frac{1-p}{2-p}u_s^2\right)$$

$$(29)$$

for $x = s_1(t)$ the interpolated point. The last derivative will be used for the Stefan equation. Analogously for the derivative of the liquid temperature profile we can substitute

a_j	$u(a_j)$
$a_0 = (i-1)dx$	$u_l^{i-1} = u_l^{n_l-1}$
$a_1 = idx$	$u_l^i = u_l^{n_l}$
$a_2 = (i+p)dx$	u_B

obtaining

$$\frac{\partial^2 u_l}{\partial x^2} = \frac{2}{dx^2} \left(\frac{u_l^{n_l-1}}{p+1} - \frac{u_l^{n_l}}{p} + \frac{u_B}{p(p+1)} \right) \quad (30)$$

for $x = idx$, the last node of the liquid domain, and

$$\frac{\partial u_l}{\partial x} = \frac{1}{dx} \left(\frac{p}{p+1} u_l^{n_l-1} - \frac{(p+1)}{p} u_l^{n_l} + \frac{2p+1}{p(p+1)} u_B \right)$$

$$(31)$$

for $x = (i+p)dx$, the interpolated point. Equation (28) should be used for the first node of the mesh, and Eq. (30) for the last node of the mesh. Equations (29) and (31) are to be used in Eq. (16). These substitutions produce the finite difference equations that are calculated at every step $s_1(kd\tau)$. Writing $s_1(kd\tau) = (i + p^k)dx$ and using the first-order Euler approximation of ds/dt we can obtain

$$p^{k+1} = p^k + \frac{d\tau}{dx^2} \left(\gamma_s \frac{\partial u_s}{\partial x} - \gamma_l \frac{\partial u_l}{\partial x} \right) \quad (32)$$

This equation is valid for the solid–liquid moving boundary in Stages 2 and 3. For the liquid-vapor moving boundary the same Eq. (29), with u_l in place of u_s, can be used with Eq. (17) to obtain the final form

$$v^{k+1} = v^k + \frac{d\tau}{dx} \left(\gamma_l \frac{\partial u_l}{\partial x} + f(\tau) \right) \quad (33)$$

where v is the parameter used to track the movement of the boundary $s_2(t) = (i+v)dx$.

To manage the movement of the boundaries we update at every time step the fractional parameters p and v. Their values lie between 0 and 1, meaning the relative boundary lies between two nodes, except when $p > 1$, which means that the moving boundary passed a node. To simulate this we remove the node from the solid domain and add a node to the liquid one. Calculating $p^{k+1} = p^k - 1$ we obtain the starting p for the spatial interval dx. For the liquid–vapor boundary we simply remove one node from the liquid domain without any additional operation, following the assumption that the vapor is continuously removed from the surface. This operation requires the determination of a temperature for the new node added in the liquid domain. Lacking physical principles to address this problem (the conservation of energy has been already used for the Stefan equation and does not provide any further information), we can again use the Lagrangian interpolation of Eq. (26). Before adding the new node, with $p > 1$, we can obtain the temperature in the position

$x = (i+1)dx$ using the information at nodes $(i-1)dx$ (where $u = u_l^{n_l-1}$), idx (where $u = u_l^{n_l}$), and $(i+p)dx$ (where $u = u_B$ by definition of s_1) obtaining:

$$u_l^{i+1,k} = \frac{1-p}{1+p} u_l^{i-1,k} + \frac{2(p-1)}{p} u_l^{i,k} + \frac{2}{p(p+1)} u_B$$

$$(34)$$

This is not a strict condition. The space and time steps are usually small, so it happens that u_l^{i+1} is very close to u_B. We verified that imposing the condition $u_l^{i+1} = u_B$ does not change the result of the simulation if the total simulation time is not close to τ_1.

THERMAL MODEL VALIDATION

To validate the code we used both an analytical solution and a test case found in the literature. Analytical solutions are very difficult to find and are only available for simple problems. For this reason we tested a simpler version of the code with only solid and liquid phases.

Analytical Solution: The Neumann Solution

The similarity solution originally obtained by Frank Neumann in 1860 for the solidification of a liquid phase can also be used for the inverse process. It is based on a particular solution of the heat equation that can be written in terms of error functions.

The problem considered is described by Eqs. (1)–(3) without taking into account the heat generation terms and with boundary and initial conditions:

$$T_l = T_0 \qquad \text{for} \quad X = 0, t \geqslant 0 \quad (35)$$

$$T_s = T_i \qquad \text{for} \quad X = \infty, t \geqslant 0 \quad (36)$$

$$T_l = T_s = T_m \quad \text{for} \quad X = S_1(t), t \geqslant 0 \quad (37)$$

Following the known resolution described by Crank [2] with some variations, verified by comparison with the Gupta [15] work, we can give the solution of Eqs. (1) and (2) as

$$T_l = T_0 + A \, \mathrm{erf} \left(\frac{X_l}{2\sqrt{\alpha_l t}} \right) \quad (38)$$

$$T_s = T_i + B \, \mathrm{erfc} \left(\frac{X_s}{2\sqrt{\alpha_s t}} \right) \quad (39)$$

Let $S_1(t)$ be given by

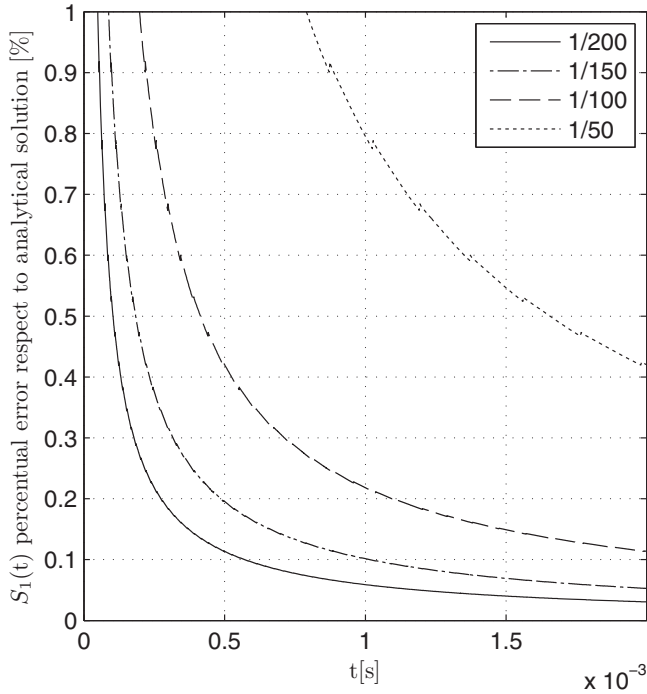$$S_1(t) = 2\lambda \sqrt{\alpha_l t}$$

Figure 4 Percent error of our calculated $S_1(t)$ with respect to Neumann's analytical solution. Error is provided for different mesh sizes; the legend shows the mesh size with respect to the total length of the slab.

where λ is an unknown constant. For $X = S_1(t)$, Eqs. (38) and (39) are equal to T_m for the boundary condition. Hence, with the previous definition of $S_1(t)$,

$$A = \frac{T_m - T_0}{\text{erf}(\lambda)}$$

$$B = \frac{T_m - T_i}{\text{erfc}\left(\lambda\sqrt{\frac{\alpha_l}{\alpha_s}}\right)}$$

Now, taking the derivatives of Eqs. (38) and (39) and inserting into Eq. (3) with the obtained values of A and B, we finally obtain

$$\frac{\exp(-\lambda^2)}{\text{erf}(\lambda)} + \frac{k_s}{k_l}\frac{(T_m - T_i)}{(T_m - T_0)}\sqrt{\frac{\alpha_l}{\alpha_s}}\frac{\exp\left(-\lambda^2\frac{\alpha_l}{\alpha_s}\right)}{\text{erfc}\left(\lambda\sqrt{\frac{\alpha_l}{\alpha_s}}\right)} = -\frac{C_m\lambda\sqrt{\pi}}{c_l(T_m - T_0)} \tag{40}$$

Calculating λ from Eq. (40) with a numerical or graphical method we obtain the final time-dependent temperature profile and the movement of the boundary.

Figure 4 shows the convergence of the numerical solution to the analytical one. Except at the very beginning of the simulation where it is not possible to start from zero for initialization issues, the difference between the two solutions quickly drops to less than 1% even with the biggest mesh size. This means that the accuracy of the calculation always grows in time, and the solution does not diverge.
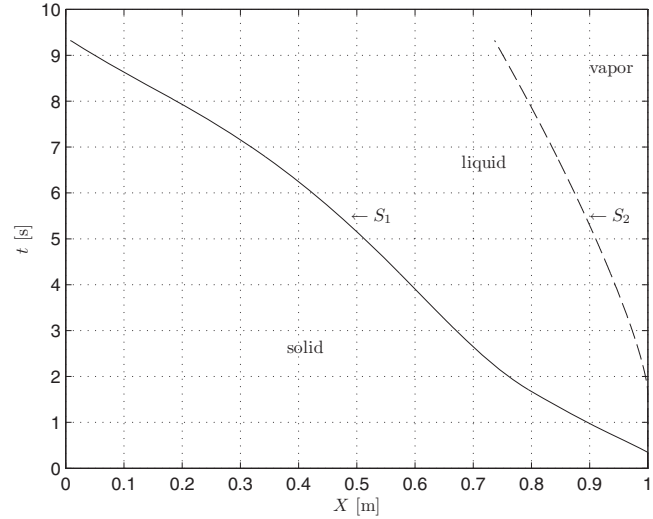

Figure 5 Our code simulation of Bonnerot's numerical problem: showing appearance, movement, and disappearance of the free boundaries on the $x - t$ plane. Solid, liquid, and vapor phase appear at increasing t. Heat flux is applied at $x = 1$.

Comparison with Previous Numerical Solution

Bonnerot and Jamet [5] proposed a solution for a two-phase Stefan problem using a finite-element method; they also modeled the appearance and disappearance of new phases. Our code has been modified to enforce an adiabatic condition at the end of the slab, as in the considered paper. The physical values used are:

$T_m = 1454\ K$	$T_v = 3000\ K$
$T_0(X) = T_0 = 27\ K$	$F(t) = F = 2500\ W/m^2$
$c_l = c_s = 1.7848\ J/(kgK)$	$\rho = 2.77\ kg/m^3$
$a = 1\ m$	$k_s = 0.259\ W/(mK)$
$k_l = 0.259\ W/(mK)$	$C_m = 779.8\ J/kg$
$C_v = 13430\ J/kg$	

The results obtained for the boundary movement $S_1(t)$ and $S_2(t)$ are shown in Figures 5 and 6. The comparison with the code of Bonnerot and Jamet [5] is shown in Figures 7 and 8 where the ratio between the values of the two solutions is plotted versus the time t. It is easy to observe that the two methods produced the same results, that is, a ratio close to 1, with a difference smaller than 3%, except where one of the two values is close to zero because of the numerical imposition of the boundary conditions (slab thickness and axis origin). This pushes the ratio toward higher yet nonphysical values.

Comparison with Previous Numerical Solution

Another comparison with previous literature was carried out with the work of Belkin [16]. His experimental data can be normalized in order to obtain a self-similar curve of a dimensionless ejected mass independent of the heat flux incoming on
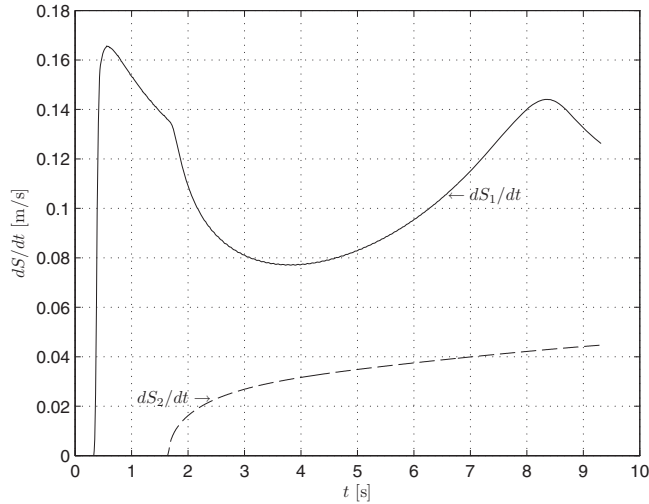
Figure 6 Our code simulation of Bonnerot's numerical problem: velocities of the free boundaries dS_1/dt and dS_2/dt plotted vs. time.

the surface, while eliminating the dependence on the total time of the arc discharge. This allows us also to validate our model from the point of view of the vaporization process:

$$M_l^* = \frac{M_l}{\frac{Q_b}{c_s T_m}}$$

$$M_v^* = \frac{M_v}{\frac{Q_b}{c_l T_m}}$$

$$\left[q_b\sqrt{t_d}\right]^* = \frac{q_b\sqrt{t_d}}{T_m\sqrt{c_l \rho k_l}}$$

where M_l^* and M_v^* are the liquid and vapor nondimensional ejected mass, and t_d is the total discharge time during which the flux q_b is assumed constant.

Figure 9 shows the nondimensional mass flow rates for liquid and vapor phase, evaluated by our code, plotted versus a nondimensional parameter $\left[q_b\sqrt{t_d}\right]^*$ that is a function of the heat flux and the discharge time. The results are quite similar to those that can be found in reference 16. Belkin identifies the onset of fusion as

$$\left[q_b\sqrt{t_d}\right]^* = \sqrt{\pi/4} = 0.885$$

According to him, at low fluxes the metal is heated to fusion conditions at shallow depths and heat is transported deeper into the metal by thermal diffusivity. For high heat flux, that is, large $\left[q_b\sqrt{t_d}\right]^*$, there is an intense vaporization of the surface and only a fraction of the energy is carried by conduction. Almost all the input energy is consumed by the vaporization of nearly all of the fused metal, leading to a small difference between M_l^* and M_v^*. In our result, $\left[q_b\sqrt{t_d}\right]^*$ is about 0.7, which is close to Belkin's value.

It is interesting to note that the maximum of the M_l^* curve, and so the onset of vaporization, can vary strongly with the imposed vapor temperature T_v. This means such a self-similarity
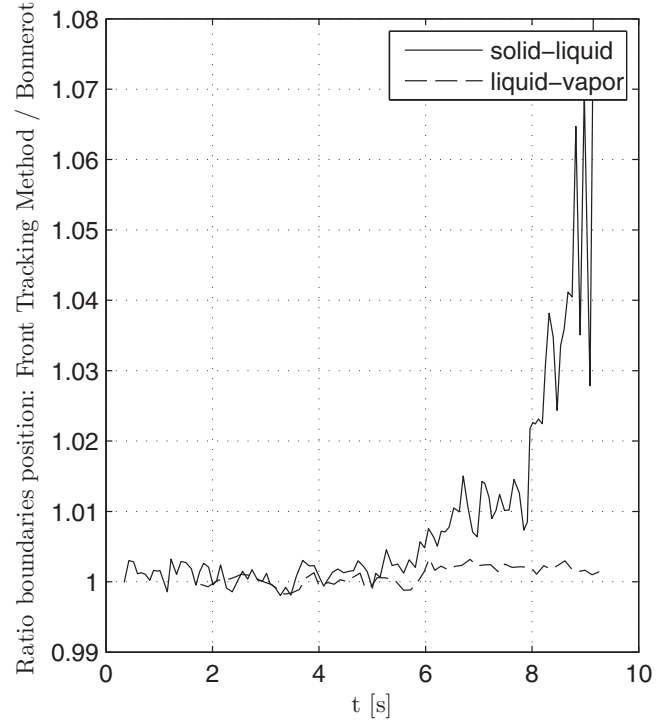

Figure 7 Comparison between our code and Bonnerot's code. Ratios of the boundary positions S_1 (continuous line) and S_2 (dashed line) with respect to time calculated with our code and Bonnerot's code.
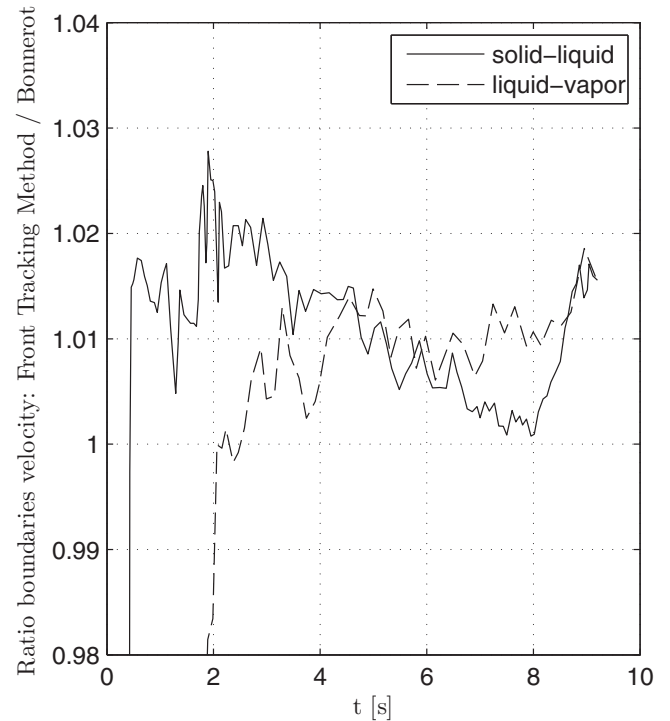

Figure 8 Comparison between our code and Bonnerot's code. Ratios of the velocities of the free boundaries dS_1/dt (continuous line) and dS_2/dt (dashed line) with respect to time calculated with our code and Bonnerot's code.
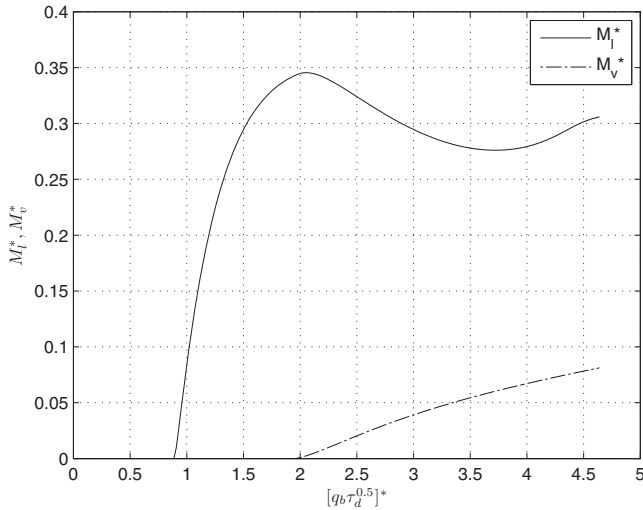
Figure 9 Results of our code. Normalization of copper simulation results according to Belkin method for evaluating experimental data.

is not maintained if pressure varies during the experiment, because of the boiling point variation. Belkin [16] developed an approximate expression for M_l^* valid within the range $55 \times 10^9 - 5 \times 10^{11} \mathrm{W/m^2}$:

$$M_{l\,approx}^* = \frac{1.3}{[q_b\sqrt{\tau_d}]^*}\left[1 - \frac{0.885}{[q_b\sqrt{\tau_d}]^*}\right]$$

which is only valid for one pressure. Nevertheless, some authors [13, 17] refer to this expression when calculating electrode evaporation without concern for this limitation.

CONCLUSIONS

The numerical solution of a one-dimensional, three-phase Stefan problem with a low Stefan number has been presented. The fundamental equations governing the phenomenon and the numerical approach used to solve the problem have been described. The results are in agreement with a previous solution obtained with a different numerical method and with experimental data found in literature.

NOMENCLATURE

a	length of the slab (m)
A	coefficient of the Neumann analytical solution
B	coefficient of the Neumann analytical solution
c_s	specific heat of solid (J/kg-K)
c_l	specific heat of liquid (J/kg-K)
C_m	latent heat of melting (J/kg)
C_v	latent heat of vaporization (J/kg)
i	integer index of the domain mesh
$f(\tau)$	dimensionless inbound heat flux in Stefan equation
$f_l(\tau)$	dimensionless inbound heat flux in boundary condition for liquid phase

$f_s(\tau)$	dimensionless inbound heat flux in boundary condition for solid phase
$F(t)$	inbound heat flux (W/m²)
g_l	dimensionless heat generation term in liquid
g_s	dimensionless heat generation term in solid
j	current density (A/m²)
k	integer index for simulation time-step progression
$\tilde{k}$	ratio of solid and liquid thermal conductivities
k_l	thermal conductivity of liquid (W/m-K)
k_s	thermal conductivity of solid (W/m-K)
M_l	melted mass (kg)
M_v	vaporized mass (kg)
p	fractional parameter for the s_1 tracking
q_b	inbound heat flux (W/m²)
q_r	radiative heat flux (W/m²)
Q_b	inbound energy provided during t_d (W)
r	arbitrary characteristic length (m)
r_d	diffusion length (m)
s_1	dimensionless position of the solid–liquid interface
s_2	dimensionless position of the liquid–vapor interface
S_1	dimensional position of the solid–liquid interface (m)
S_2	dimensional position of the liquid–vapor interface (m)
Ste	Stefan number
t	time (s)
t_d	characteristic time of the phenomenon, i.e. discharge time (s)
T_i	initial system temperature (anode and environment) (K)
T_l	liquid temperature (K)
T_m	melting temperature (K)
T_s	solid temperature (K)
T_{surf}	temperature of the surface exposed to vapor phase (K)
T_v	vaporization temperature (K)
u_B	dimensionless melting temperature
u_l	dimensionless liquid temperature
u_s	dimensionless solid temperature
u_v	dimensionless vapor temperature
v	fractional parameter for the s_2 tracking
x	dimensionless spatial coordinate
x_l	dimensionless spatial coordinate for the liquid domain
x_s	dimensionless spatial coordinate for the solid domain
X	dimensional spatial coordinate (m)
X_l	dimensional spatial coordinate for the liquid domain (m)
X_s	dimensional spatial coordinate for the solid domain (m)

Greek Symbols

α_s	diffusivity of solid (m²/s)
α_l	diffusivity of liquid (m²/s)
γ_l	dimensionless multiplier proportional to Ste
γ_{lv}	dimensionless multiplier proportional to λ_v
ϵ	emissivity
η_s	resistivity of solid (Ω−m)
η_l	resistivity of liquid (Ω−m)
λ_v	ratio of sensible heat of solid and latent heat of vaporization

ρ   density (kg/m³)
τ   dimensionless time

REFERENCES

[1] Carslaw, H. S., and Jaeger J. C.,*Conduction of Heat in Solids,* 2nd ed., Oxford University Press, Oxford,UK, 1959.

[2] Crank, J., *Free and Moving Boundary Problems*, Oxford University Press, Oxford,UK, 1984.

[3] Kharab, A., Spreadsheet Simulation of the Moving Boundary of the One-Phase Stefan Problem, *Computer Methods in Applied Mechanics and Engineering*, vol. 145, pp. 217–225, 1997.

[4] Atthey, D. R., A Finite Difference Scheme for Melting Problems, *IMA Journal of Applied Mathematics*, vol. 13, pp. 353–366, 1974.

[5] Bonnerot, R., and Jamet, P., A Conservative Finite Element Method for One Dimensional Stefan Problems With Appearing and Disappearing Phases, *Journal of Computational Physics*, vol. 41, pp. 357–388, 1981.

[6] Javierre, E., Vuik, C., Vermolen, F. J., and Segal, A., A Level Set Method for Three Dimensional Vector Stefan Problems: Dissolution of Stoichiometric Particles in Multi-Component Alloys, *Journal of Computational Physics*, vol. 224, no. 1, pp. 222–240, 2007.

[7] Muradoglu, M., and Tryggvason, G., A Front-Tracking Method for Computation of Interfacial Flows with Soluble Surfactants, *Journal of Computational Physics*, vol. 227, no. 4, pp. 2238–2262, 2008.

[8] Pang, S., Chen, L., Zhou, J., Yin, Y., and Chen, T., A Three-Dimensional Sharp Interface Model for Self-Consistent Keyhole and Weld Pool Dynamics in Deep Penetration Laser Welding, *Journal of Physics D: Applied Physics*, vol. 44, no. 2, pp. 025301–025315, 2011.

[9] Somerville, J. M., Blevin, W. R., and Fletcher, N. H., Erode Phenomena in Transient Arcs, *Proceedings of the Physical Society*, vol. 65, no. 12-B, pp. 963–970, 1952.

[10] Somerville, J. M., and Grainger, C. T., Current Distribution in an Expanding Spark Channel, *British Journal of Applied Physics*, vol. 7, pp. 109–110, 1956.

[11] Somerville, J. M., and Williams, J. F., The Early Stages of Spark Channel Expansion, *Proceedings of the Physical Society*, vol. 74, no. 3, pp. 309–315, 1959.

[12] Beilis, I. I., State of the Theory of Vacuum Arcs, *IEEE Transactions on Plasma Science*, vol. 29, no. 5, pp. 657–670, 2001.

[13] Lehr, F. M., and Kristiansen, M., Electrode Erosion from High Current Moving Arcs, *IEEE Transactions on Plasma Science*, vol. 17, no. 5, pp. 811–817, 1989.

[14] Özisik, M. N., *Heat Conduction*, John Wiley and Sons, New York, NY, 1980.

[15] Gupta, S. C., *The Classical Stefan Problem. Basic Concepts, Modelling and Analysis*, North Holland Series in Applied Mathematics and Mechanics, Elsevier, AmsterdamThe Netherlands, 2003.

[16] Belkin, G. S., Dependence of Electrode Erosion on Heat Flux and Duration of Current Flow, *Soviet Physics—Technical Physics*, vol. 15, no. 7, pp. 1167–1170, 1971.

[17] Borkowsky, P., and Hasegawa, M., A Computer Program for the Calculation of Electrode Mass Loss Under Electric Arc Conditions, *IEEE Transactions on Electron Devices*, vol. E90-C, no. 7, pp. 1369–1376, 2007.

Guido Parissenti graduated in Space Engineering at Politecnico di Milano in 2008. He was a Visiting Student Research Collaborator at the Electric Propulsion and Plasma Dynamic Laboratory (EPPDyLs) at Princeton University (Princeton, NJ) where he performed his M.Sc. Thesis on the topic of anode erosion due to spots formation on MPD Thrusters. He is presently attending his Ph.D. degree in Energetic at Politecnico di Milano about industrial plasma applications in waste treatment and recovery.

Alfonso Niro graduated in Nuclear Engineering in 1982 at Politecnico di Milano where he also received his Ph.D. in 1987; during 1988, he was a visiting scientist at MIT, (Cambridge, MA), within a NATO-CNR grant. In 1990 he started his academic career as an Assistant Professor and he became an Associate Professor in 1997. Since 2001 he has been a Full Professor of Thermodynamics and Heat Transfer. His major research interests are in the field of Heat Transfer and Engineering Thermodynamics. His studies in heat transfer are concerned with both single-phase flows and two-phase flows, flow-boiling and convective condensation of halo-refrigerants inside microfin tubes, critical heat flux in micro-channels, pool-boiling instabilities at low pressure. To these subjects he has contributed with more than 80 scientific papers.